The Impact of Dark Matter on the Related Sector of the Scotogenic Model and Its Implications

Gaber Faisel, Mohammed Ismael, and Maladh Alanssari

Department of Physics, Faculty of Arts and Sciences, Suleyman Demirel University, 32260 Isparta, Turkey

Abstract

We investigate the impact of the recent results concerning the fit to the global data on neutrino oscillations, the direct detection experiments of the dark matter, and the Planck measurement for the relic density on the parameter space relevant to the fermionic dark matter sector of the scotogenic model. In this sector, the lightest new singlet fermion is adopted to be the dark matter candidate. We show that masses of dark matter and new scalars smaller than or equal to 1 TeV satisfying the strongest constraints arise from $\frac{|\Delta m^2_{31}|}{\Delta m^2_{21}}$, $\mu \to e\gamma$, and direct detection constraints do not guarantee that $\Omega\hat{h}^2$ lies in the 2σ range provided recently by the Planck satellite measurements with $\Delta m^2_{ij} = m^2_i - m^2_j$. This result is valid for the case that the lightest new singlet fermion N_1 is the dark matter candidate and for the scenarios of normal and inverted ordering of neutrino masses. Moreover, we find that if N_1 is degenerate or nearly degenerate in mass with the next lightest singlet fermion N_2, the new contributions from coannihilation of N_1 and N_2 become relevant to reduce the values of the Yukawa coupling needed for producing the relic density of dark matter within 2σ range of its measured value while respecting the imposed constraints.

Keywords: scotogenic model, dark matter, neutrino masses
DOI: 10.31526/LHEP.2023.374

1. INTRODUCTION

One of the important issues related to the structure of our Universe is the so-known Dark Matter (DM). It accounts for almost 27% of the matter in our universe. The combined analysis of the Planck satellite 2018 results [1] leads to a value $\Omega\hat{h}^2 = 0.120 \pm 0.001$ where $\hat{h}$ is the Hubble parameter and Ω denotes the present DM density relative to its critical value.

The DM candidate has to be a stable particle in addition to not having direct interactions with the strong and electroweak forces. The stability of DM can be assured by the implementation of discrete or continuous symmetry. The DM candidate must be nonrelativistic, i.e., cold. The other possibility that DM can be hot is excluded by many observations.

The first hint for the presence of DM was remarked in the thirties of the last century [2], and since then, many observations supported its existence. However, up to date, attempts to observe a candidate for DM in many proposed experiments fail to achieve this goal.

The fact that the standard model (SM) does not have a viable candidate to play the role of DM motivated to extend the SM through enlarging either the gauge group structure or the matter content or both of them. One of the simple extensions of the SM is the Scotogenic Model [3] which permits the generation of neutrino masses while providing a DM candidate that can be any one of the new particles in the model. Thus, it can be one of (η, N_i) where η is a new scalar doublet and $N_{1,2,3}$ are three singlet Majorana fermions [3]. The DM in the scotogenic model and in many extended versions of the model has been investigated in [4, 5, 6, 7, 8]. Moreover, prospects for searches at Collider have been subjected to many studies as in [6, 9, 10].

The paper is organized as follows: in Section 2, we give a brief review of the structure of the scotogenic model, neutrino mass generation in the model, fermionic DM sector of the model, and relevant constraints on the parameter space of the model. In Section 3, we present our analysis and results.

2. THE SCOTOGENIC MODEL

The scalar sector of the scotogenic model contains two scalar doublets, namely, Φ and η with Φ representing the usual SM Higgs doublet. The interactions of these scalars with the gauge bosons and with each other can be derived from the following Lagrangian:

$$\mathcal{L} = (\mathcal{D}^\mu \Phi)^\dagger \mathcal{D}_\mu \Phi + (\mathcal{D}^\mu \eta)^\dagger \mathcal{D}_\mu \eta - \mathcal{V}, \tag{1}$$

where $\mathcal{D}_\mu$ is the familiar covariant derivative constructed using the SM gauge fields and the expression of the scalar potential $\mathcal{V}$ can be found in [3]. After electroweak symmetry breaking, we have $\Phi = \left(0 \ \frac{1}{\sqrt{2}}(h+v)\right)^{\mathrm{Tr}}$ and $\eta = \left(H^+ \ \frac{1}{\sqrt{2}}(\mathcal{S} + i\mathcal{P})\right)^{\mathrm{Tr}}$, where Tr stands for transpose, h is the physical Higgs boson, and v is the vacuum expectation value (VEV) of Φ. Because of the Z_2 symmetry, the VEV of η is zero. The masses of $\mathcal{S}$, $\mathcal{P}$, and $H^\pm$ are then given by $m^2_{\mathcal{S}} = m^2_{\mathcal{P}} + \lambda_5 v^2 = \mu^2_2 + \frac{1}{2}(\lambda_3 + \lambda_4 + \lambda_5)v^2$ and $m^2_H = \mu^2_2 + \frac{1}{2}\lambda_3 v^2$ [11]. We make the usual assumption that λ_5 is small, $|\lambda_5| \ll |\lambda_3 + \lambda_4|$, implying that $m_{\mathcal{S},\mathcal{P}}$ are nearly degenerate, $|m^2_{\mathcal{S}} - m^2_{\mathcal{P}}| = |\lambda_5| v^2 \ll m^2_{\mathcal{S}} \simeq m^2_{\mathcal{P}}$. The Lagrangian describing the masses and interactions of N_k is given as

$$\begin{aligned}\mathcal{L}_N = &-\frac{1}{2} M_k \overline{N^c_k} P_R N_k \\ &+ Y_{rk}\left[\bar{\ell}_r H^- - \frac{1}{\sqrt{2}}\bar{\nu}_r\left(\mathcal{S} - i\mathcal{P}\right)\right] P_R N_k + \text{H.c.},\end{aligned} \tag{2}$$

where $\ell_{1,2,3} = e, \mu, \tau$, Y_{rk} and M_k stand for the Yukawa couplings and masses of N_k, the superscript c refers to the charge conjugation, the chirality operator is defined as $P_R = \frac{1}{2}(1+\gamma_5)$, and $k, r = 1, 2, 3$.

2.1. Neutrino Mass Generation

In the scotogenic model, neutrino masses are absent at the tree level as a consequence of the Z_2 symmetry imposed on the

model. However, neutrino mass can be generated radiatively at the one-loop level through $\mathcal{S}$, $\mathcal{P}$, and N_k that mediate internally the relevant loop diagrams. The mass eigenvalues m_j can be expressed as $\mathrm{diag}(m_1, m_2, m_3) = \mathcal{U}^\dagger \mathcal{M}_\nu \mathcal{U}^*$ [3]:

$$\begin{aligned} \mathcal{M}_\nu &= Y\,\mathrm{diag}\left(\Lambda_1, \Lambda_2, \Lambda_3\right) Y^{\mathrm{T}}, \\ \Lambda_k &= \frac{\lambda_5 v^2}{16\pi^2 M_k}\left[\frac{M_k^2}{m_0^2 - M_k^2} + \frac{2M_k^4 \ln\left(M_k/m_0\right)}{\left(m_0^2 - M_k^2\right)^2}\right]. \end{aligned} \tag{3}$$

Here, $m_0 = \frac{1}{2}(m_{\mathcal{S}} + m_{\mathcal{P}})$, $\mathcal{U}$ is the familiar Pontecorvo-Maki-Nakagawa-Sakata (PMNS) unitary matrix, and the expression of Λ_k corresponds to the adopted approximation $m_0 \simeq m_{\mathcal{S}} \simeq m_{\mathcal{P}}$ case. Regarding the matrix $\mathcal{U}$, we adopt the PDG parametrization [12] $\mathcal{U} = \tilde{u}\,\mathrm{diag}(e^{i\alpha_1/2}, e^{i\alpha_2/2}, 1)$ with $\alpha_{1,2} \in [0, 2\pi]$ expressing the Majorana CP-violation phases. The matrix $\tilde{u}$ can be written in terms of a Dirac phase $\delta \in [0, 2\pi]$, $c_{mn} = \cos\theta_{mn} \geq 0$, and $s_{mn} = \sin\theta_{mn} \geq 0$. The explicit form of $\tilde{u}$ is given in equation (10) in [13]. In our calculations, we consider the analytic expressions of $Y_{\ell_r k}$ given in [11] as

$$\begin{aligned} Y_{e1} &= \frac{-c_{12}c_{13}Y_1}{c_{12}c_{23}s_{13}e^{i\delta} - s_{12}s_{23}}, \quad Y_{e2} = \frac{-s_{12}c_{13}Y_2}{s_{12}c_{23}s_{13}e^{i\delta} + c_{12}s_{23}}, \\ Y_{\mu 1} &= \frac{\left(c_{12}s_{23}s_{13}e^{i\delta} + s_{12}c_{23}\right)Y_1}{c_{12}c_{23}s_{13}e^{i\delta} - s_{12}s_{23}}, \quad Y_{\mu 3} = \frac{s_{23}Y_3}{c_{23}}, \quad Y_{\tau k} = Y_k, \\ Y_{e3} &= \frac{s_{13}Y_3}{c_{23}c_{13}e^{i\delta}}, \quad Y_{\mu 2} = \frac{\left(s_{12}s_{23}s_{13}e^{i\delta} - c_{12}c_{23}\right)Y_2}{s_{12}c_{23}s_{13}e^{i\delta} + c_{12}s_{23}}. \end{aligned} \tag{4}$$

These solutions correspond to the neutrino mass eigenvalues [11]:

$$m_1 = \frac{\Lambda_1 Y_{e1}^2 e^{-i\alpha_1}}{c_{12}^2 c_{13}^2}, \quad m_2 = \frac{\Lambda_2 Y_{e2}^2 e^{-i\alpha_2}}{s_{12}^2 c_{13}^2}, \quad m_3 = \frac{\Lambda_3 Y_3^2}{c_{13}^2 c_{23}^2}. \tag{5}$$

The masses $m_{1,2,3}$ must be real and nonnegative. Consequently, one obtains [11]

$$\alpha_1 = \arg\left(\Lambda_1 Y_{e1}^2\right), \quad \alpha_2 = \arg\left(\Lambda_2 Y_{e2}^2\right), \quad \arg\left(\Lambda_3 Y_3^2\right) = 0 \tag{6}$$

in a consistency with the neutrino oscillation data.

2.2. Dark Matter

As a consequence of the Z_2 symmetry in which only nonstandard model particles are odd under this symmetry, the lightest odd particle is stable and thus it becomes a dark matter candidate. In our investigation, we consider a scenario in which the lightest Majorana singlet fermion, N_1, is the dark matter particle. The dominant contributions to the annihilation cross-section σ_{ann} originate from the tree-level processes $N_1\bar{N}_1 \to \ell_i^-\ell_j^+$ and $N_1\bar{N}_1 \to \nu_i\bar{\nu}_j$ mediated by the exchange of $H^\pm$ and $(\mathcal{S}, \mathcal{P})$, respectively. The obtained annihilation cross-section can be expanded in terms of the relative speed v_{rel} of the $N_1\bar{N}_1$ pair in their center-of-mass frame as $\sigma_{\mathrm{ann}} v_{\mathrm{rel}} = a + b v_{\mathrm{rel}}^2 + \mathcal{O}(v_{\mathrm{rel}}^4)$. The relic density Ω can be expressed in terms of a and b as [14]

$$\begin{aligned} \Omega\hat{h}^2 &= \frac{1.07 \times 10^9 x_f\,\mathrm{GeV}^{-1}}{\sqrt{g_*}\, m_{\mathrm{Pl}}\left[a + 3(b - a/4)/x_f\right]}, \\ x_f &= \ln\frac{0.0764 c(2+c)\left(a + 6b/x_f\right) M_1 m_{\mathrm{Pl}}}{\sqrt{g_* x_f}}, \end{aligned} \tag{7}$$

where $c \simeq 1/2$, $m_{\mathrm{Pl}} = 1.22 \times 10^{19}$ GeV is the Planck mass, g_* is the number of relativistic degrees of freedom below the freeze-out temperature $T_f = M_1/x_f$, and $\hat{h}$ denotes the Hubble parameter. The expressions of a and b can be found in [15].

In [16], it was pointed out that when the DM and the new scalar particle are degenerate in mass, their coannihilation processes become important for the DM relic density. Consequently, in order to compensate for DM relic density, the dark matter particle has to be heavier which in turn yields more small $\mathrm{BR}(\mu \to e\gamma)$ and consequently strong constraints [17]. As a result, to avoid the stringent constraints on the parameter space, we choose $M_1 < m_0$ to cancel the possibility of the coannihilation of new scalar particles and DM. Besides, we consider the case in which the lightest and next to lightest singlet fermions N_1 and N_2 are degenerate in masses and play the role of the DM. We refer to [5, 13, 16] for more discussions and details about this case.

2.3. Constraints

In our calculations, we consider the two known scenarios for neutrino masses, namely, the normal ordering (NO) and the inverted ordering (IO) scenarios. Various measurements can be used to obtain information on the values of some of the neutrino parameters. In our analysis, we use the results of the recent fit to the global data on neutrino oscillations presented in [18].

Concerning the cosmological limits on the sum of the neutrino masses, the tightest 2σ bound taking into account CMB temperature, polarization, and lensing measurements from the Planck satellite, BAO observations, $H(z)$ information, and Supernovae Ia data constraint $\sum m_i < 0.12\,\mathrm{eV}$, neutrinoless double beta decay experiments can set constraints on the quantity $\langle m\rangle_{ee}$ defined as $\langle m\rangle_{ee} = m_1\mathcal{U}_{e1}^2 + m_2\mathcal{U}_{e2}^2 + m_3\mathcal{U}_{e3}^2$. The upper limit reads $|\langle m\rangle_{ee}| < 0.06$–$0.2\,\mathrm{eV}$ at the 95% confidence level [19]. Accordingly, in our analysis, we require the relevant parameter space to satisfy the bound $|\langle m\rangle_{ee}| < 0.06\,\mathrm{eV}$. Additionally, using the results of the recent fit to global data on neutrino oscillations, we require $32.0 < \frac{|\Delta m_{31}^2|}{\Delta m_{21}^2} < 36.0$ and $30.75 < \frac{|\Delta m_{31}^2|}{\Delta m_{21}^2} < 34.66$ in the NO and IO scenarios, respectively, based on the 90% CL ranges of the data on $|\Delta m_{31}^2|$ and Δm_{21}^2.

The Yukawa interactions can lead to lepton flavor violation (LFV) processes as discussed in detail in [20]. The current experimental limits on an important class of LFV processes are $\mathrm{BR}(\mu \to e\gamma) < 4.2 \times 10^{-13}$ [21], $\mathrm{BR}(\tau \to e\gamma) < 3.3 \times 10^{-8}$ [22], and $\mathrm{BR}(\tau \to \mu\gamma) < 4.4 \times 10^{-8}$ [22]. The expressions of the branching ratios can be found in [20]. The flavor-diagonal counterpart of the previous FLV processes leads to a modification of the anomalous magnetic moment a_{ℓ_i} of the lepton ℓ_i

given by [23]

$$\Delta a_{\ell_i} = \frac{-m_{\ell_i}^2}{16\pi^2 m_H^2} \sum_k |Y_{ik}|^2 \mathcal{F}\left(M_k^2/m_H^2\right). \quad (8)$$

Among these, the anomalous magnetic moment a_μ can lead to stringent bounds on the scotogenic parameter space. Currently, the difference between the SM and the experimental values of a_μ is given by $a_\mu^{\rm exp} - a_\mu^{\rm SM} = (2.51 \pm 0.59) \times 10^{-9}$ [24].

For the DM candidate N_1, the interactions with nucleons appear at the one-loop level. As already discussed in [25], the spin-independent cross-section resulted from the Higgs exchange. We follow [25, 26] and set the couplings $\lambda_{3,4} = 0.01$ to avoid the strong constraints from direct detection [27, 28]. Consequently, from the discussion about scalar masses above, we find that $m_{\mathcal{S}} \simeq m_{\mathcal{P}} \simeq m_{H^\pm} + \frac{1}{2}\lambda_4 v^2 \simeq m_{H^\pm} + 350\,\text{GeV}$. It should be noted that the strong constraints from the direct detection were not studied before in [11, 15]. A closer look at the given sets of the benchmark points listed in these references reveals that these benchmark points do not respect the strong constraints from the direct detection that require picking $m_0 \simeq m_{\mathcal{S}} \simeq m_{\mathcal{P}} \simeq m_{H^\pm} + 350$. Additionally, in this work we use the latest neutrino oscillation parameters determined from the global analysis given in [18]. This in turn leads to different values of the Yukawa couplings listed in equation (4) except for the last line in the equation. As a result, this change will affect the parameter space respecting the studied constraints and accordingly predictions of the model presented in [11, 15]. For instance, if we take one of the allowed benchmark points in [11] $\{Y_1, Y_2, Y_3, M_1, M_2, M_3, m_{H^\pm}\} \equiv \{0.155, 0.380, 0.712, 20, 29, 85, 70\}$ and using the latest global fit for neutrino data in [18], one finds that it leads to the prediction $\text{BR}(\mu \to e\gamma) \simeq 2.05 \times 10^{-6}$, which violates the experimental bound imposed on $\text{BR}(\mu \to e\gamma)$. Finally, we will discuss, in this work, the impact of considering the IO neutrino mass scenario on the allowed parameter space by the set of the relevant constraints discussed above. This investigation was not carried out in [11, 15].

3. RESULTS AND DISCUSSIONS

We start our analysis by setting $\theta_{12,23,13}$ and δ to their central values listed in the recent fit to the global data on neutrino oscillations [18], and perform scanning over the related parameter space of the model which include the masses of $N_{1,2,3}$, m_H, m_0 and the parameters $Y_{1,2,3}$ contributing to the Yukaw couplings. Experimentally, constraints can be set on the masses of the new scalars in the model using the data on W and Z widths and the null results of direct searches for new particles at e^+e^- colliders [29]. These constraints read $m_{H^\pm} + m_{\mathcal{S},\mathcal{P}} > m_{W^\pm}$, $m_{H^\pm} > 70\,\text{GeV}$, $m_{\mathcal{S}} + m_{\mathcal{P}} > m_Z$. For light dark matter masses $M_1 < 100\,\text{GeV}$, lepton flavor violation [30] and direct search at LHC [31, 32] mostly exclude the parameter space. As a consequence, we require all scalars to be above 100 GeV. Regarding the new singlet fermion masses, the mass of N_1 is not constrained by current collider data. On the other hand, the masses of the fermions N_2 and N_3 have to be large to satisfy the current lepton flavor violation. In the analysis below, we set the masses of the new particles in GeV as $M_2 = M_1 + 200$, $M_3 = M_1 + 250$, $m_H = M_1 + 400$, and $m_0 = M_1 + 750$. We start by discussing a scenario in which the lightest particle N_1 plays the role of DM.

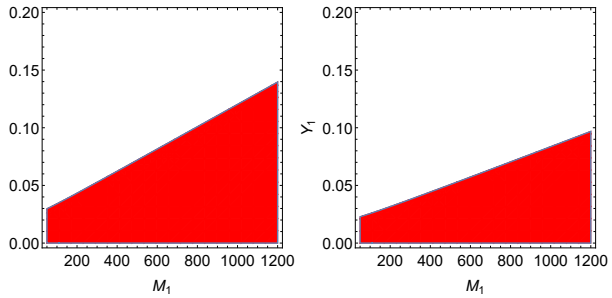

FIGURE 1: Left (Right) allowed regions in the M_1-Y_1 planes by $\mu \to e\gamma$ constraint in NO (IO) neutrino mass scenarios for $Y_2 = 0.01$ and $Y_3 = 0.03$.

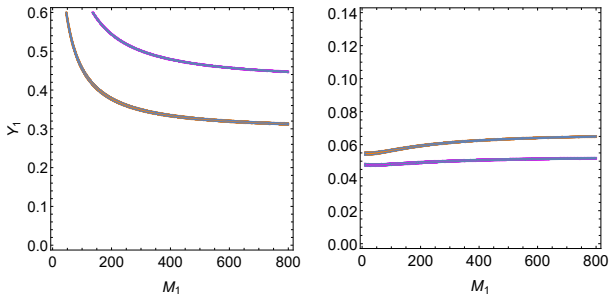

FIGURE 2: Left (right) plot: allowed regions in the M_1-Y_1 (M_1-Y_2) planes by $\frac{|\Delta m_{31}^2|}{\Delta m_{21}^2}$ constraints in NO and IO neutrino mass scenarios in magenta and orange colors, respectively. To obtain the left (right) plot, we used $Y_2 = 0.5$, $Y_3 = 0.9$ ($Y_1 = 0.04$, $Y_3 = 0.12$).

In Figure 1, we show our results for the allowed regions, red color regions, in the M_1-Y_1 plane by applying the $\mu \to e\gamma$ constraint. We have checked and confirmed that the imposed constraints on the parameter space from the processes $\tau \to e\gamma$ and $\tau \to \mu\gamma$ are weak so that not only the red regions but nearly most of the shown regions in the figures are allowed. In addition, we note from the figure that, in the NO neutrino mass scenario, larger values of Y_1 can be allowed by the $\mu \to e\gamma$ constraint which are excluded in the IO scenario.

In Figure 2, we display our results for the allowed regions in the M_1-Y_1 and M_1-Y_2 planes by $\frac{|\Delta m_{31}^2|}{\Delta m_{21}^2}$ constraints in NO and IO neutrino mass scenarios represented by magenta and orange colors, respectively. Regarding the allowed regions in the M_1-Y_1 plane, we find that, from the left plot in the figure, it is possible to get large allowed values of Y_1 in the NO neutrino mass scenario compared to the allowed ones in IO scenario for each value of M_1. This finding is reversed if we consider the M_1-Y_2 plane as can be remarked from the right plot in the figure.

In Figure 3, we show our results for the allowed regions in the M_1-Y_1 plane by $\mu \to e\gamma$, $\frac{|\Delta m_{31}^2|}{\Delta m_{21}^2}$ and $\Omega\hat{h}^2$ constraints for both NO and IO neutrino mass scenarios. Clearly from the figure, no region in the M_1-Y_1 plane satisfies the considered constraints simultaneously for the set of the other chosen parameters. One reason for this can be attributed to the large values of Y_1 required to satisfy the relic density $\Omega\hat{h}^2$ constraint as can be seen from the blue regions in the plots. It turns out that the effect of having large values of Y_1 coupling to satisfy the relic density $\Omega\hat{h}^2$ constraint can be achieved with small values of Y_1 coupling if one considers a scenario in which N_1 and N_2 are

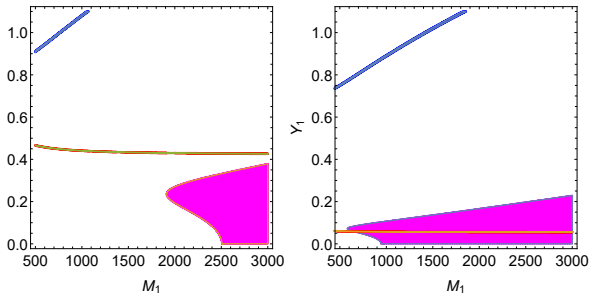

FIGURE 3: Left (Right): allowed regions in the M_1-Y_1 plane by $\mu \to e\gamma$, $\frac{|\Delta m^2_{31}|}{\Delta m^2_{21}}$, and $\Omega\hat{h}^2$ constraints in magenta, red, and blue colors, respectively, corresponding to NO (IO) scenarios. For the left plot, we set $Y_2 = 0.5$ and $Y_3 = 0.8$ while for the right plot we used $Y_2 = 0.1$ and $Y_3 = 0.2$.

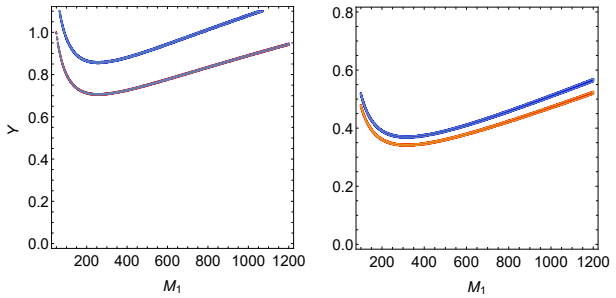

FIGURE 4: Left (Right): allowed regions in the M_1-Y_1 plane by $\Omega\hat{h}^2$ constraints for N_1 being DM candidate (N_1 being degenerate with N_2 in mass) where the regions in blue and red colors correspond to the NO and IO neutrino mass scenarios, respectively. For obtaining the right plot, we used also $Y_2 = 0.3$.

degenerate or nearly degenerate in their masses where contributions from coannihilation become relevant. This can be clear from Figure 4 in which we provide the plots in the two cases of DM: either only N_1 or a degenerate N_1 and N_2 DM. In the figure, the regions in blue and red colors correspond to the NO and IO neutrino mass scenarios, respectively. It is clearly from the figure that the mass degeneracy of N_1 and N_2 allows small values of Y_1 to satisfy the bounds from $\Omega\hat{h}^2$ measurements. This in turn leads to the possibility of finding a parameter space that can satisfy the strongest bounds from $\mu \to e\gamma$, $\frac{|\Delta m^2_{31}|}{\Delta m^2_{21}}$, $\Omega\hat{h}^2$, and the direct detection simultaneously as can be seen from the intersection of all regions representing the constraints in Figure 5. This will have an impact on the set of benchmark points obtained in [11, 15, 13] and on their corresponding predictions which requires further extensive investigation that we leave to a possible future study. It should be noted that the result in Figure 5 is just an example for illustration and one can vary the parameters to obtain other regions.

CONFLICTS OF INTEREST

The authors declare that there are no conflicts of interest regarding the publication of this paper.

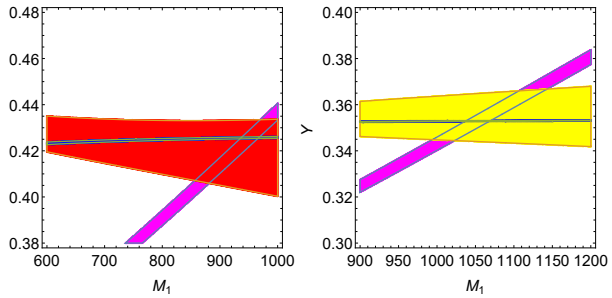

FIGURE 5: Left (Right): allowed regions in the M_1-Y_1 plane by $\mu \to e\gamma$, $\frac{|\Delta m^2_{31}|}{\Delta m^2_{21}}$, and $\Omega\hat{h}^2$ constraints in red (yellow), blue, and magenta colors, respectively, corresponding to NO (IO) scenario for $Y_2 = 0.49$ and $Y_3 = 0.66$ ($Y_2 = 0.55$ and $Y_3 = 0.6$).

References

[1] N. Aghanim et al. [Planck], "Planck 2018 results. VI. Cosmological parameters," Astron. Astrophys. **641**, A6 (2020) [erratum: Astron. Astrophys. **652**, C4 (2021)].

[2] F. Zwicky, "Die Rotverschiebung von extragalaktischen Nebeln," Helv. Phys. Acta **6**, 110–127 (1933).

[3] E. Ma, "Verifiable radiative seesaw mechanism of neutrino mass and dark matter," Phys. Rev. D **73**, 077301 (2006).

[4] D. Suematsu, T. Toma and T. Yoshida, "Reconciliation of CDM abundance and $mu \to e_\gamma$ in a radiative seesaw model," Phys. Rev. D **79**, 093004 (2009).

[5] D. Suematsu, T. Toma, and T. Yoshida, "Enhancement of the annihilation of dark matter in a radiative seesaw model," Phys. Rev. D **82**, 013012 (2010).

[6] D. Aristizabal Sierra, J. Kubo, D. Restrepo, D. Suematsu, and O. Zapata, "Radiative seesaw: Warm dark matter, collider and lepton flavour violating signals," Phys. Rev. D **79**, 013011 (2009).

[7] Y. Kajiyama, H. Okada, and T. Toma, "Direct and Indirect Detection of Dark Matter in D6 Flavor Symmetric Model," Eur. Phys. J. C **71**, 1688 (2011).

[8] Y. Kajiyama, H. Okada, and T. Toma, "A light Scalar Dark Matter for CoGeNT and DAMA in D_6 Flavor Symmetric Model," arXiv:1109.2722.

[9] M. Aoki and S. Kanemura, "Probing the Majorana nature of TeV-scale radiative seesaw models at collider experiments," Phys. Lett. B **689**, 28 (2010).

[10] D. Schmidt, T. Schwetz, and T. Toma, "Direct Detection of Leptophilic Dark Matter in a Model with Radiative Neutrino Masses," Phys. Rev. D **85**, 073009 (2012).

[11] S. Y. Ho and J. Tandean, "Probing Scotogenic Effects in e^+e^- Colliders," Phys. Rev. D **89**, 114025 (2014).

[12] J. Beringer et al. [Particle Data Group Collaboration], "Review of Particle Physics (RPP)," Phys. Rev. D **86**, 010001 (2012).

[13] G. Faisel, S. Y. Ho, and J. Tandean, "Exploring X-Ray Lines as Scotogenic Signals," Phys. Lett. B **738**, 380–385 (2014).

[14] G. Jungman, M. Kamionkowski, and K. Griest, "Supersymmetric dark matter," Phys. Rept. **267**, 195 (1996).

[15] S. Y. Ho and J. Tandean, "Probing Scotogenic Effects in Higgs Boson Decays," Phys. Rev. D **87**, 095015 (2013).

[16] T. Kitabayashi, "Primordial black holes and lepton flavor violation with scotogenic dark matter," PTEP **2022**, no.3, 033B02 (2022).

[17] T. Kitabayashi, Int. J. Mod. Phys. A **36**, 2150139 (2021).

[18] P. F. de Salas, D. V. Forero, S. Gariazzo, P. Martínez-Miravé, O. Mena, C. A. Ternes, M. Tórtola, and J. W. F. Valle, "2020 global reassessment of the neutrino oscillation picture," JHEP **02**, 071 (2021).

[19] M. Agostini et al. [GERDA], "Final Results of GERDA on the Search for Neutrinoless Double-β Decay," Phys. Rev. Lett. **125**, no.25, 252502 (2020).

[20] T. Toma and A. Vicente, "Lepton Flavor Violation in the Scotogenic Model," JHEP **01**, 160 (2014).

[21] A. M. Baldini et al. [MEG], "Search for the lepton flavour violating decay $\mu^+ \to e^+\gamma$ with the full dataset of the MEG experiment," Eur. Phys. J. C **76**, no.8, 434 (2016).

[22] B. Aubert et al. [BaBar], "Searches for Lepton flavor violation in the decays tau$\{+/-\}$ $\to$ e$\{+/-\}$gamma and tau$\{+/-\}$ $\to$ mu$\{+/-\}$gamma," Phys. Rev. Lett. **104**, 021802 (2010).

[23] E. Ma and M. Raidal, "Neutrino mass, muon anomalous magnetic moment, and lepton flavor nonconservation," Phys. Rev. Lett. **87**, 011802 (2001) [Erratum-ibid. **87**, 159901 (2001)].

[24] T. Aoyama, N. Asmussen, M. Benayoun, J. Bijnens, T. Blum, M. Bruno, I. Caprini, C. M. Carloni Calame, M. Cè, and G. Colangelo et al., "The anomalous magnetic moment of the muon in the Standard Model," Phys. Rept. **887**, 1–166 (2020).

[25] A. Ibarra, C. E. Yaguna, and O. Zapata, "Direct Detection of Fermion Dark Matter in the Radiative Seesaw Model," Phys. Rev. D **93**, no.3, 035012 (2016).

[26] J. Liu, Z. L. Han, Y. Jin, and H. Li, "Unraveling the Scotogenic Model at Muon Collider," [arXiv:2207.07382 [hep-ph]].

[27] E. Aprile et al. [XENON], "Dark Matter Search Results from a One Ton-Year Exposure of XENON1T," Phys. Rev. Lett. **121**, no.11, 111302 (2018).

[28] Y. Meng et al. [PandaX-4T], "Dark Matter Search Results from the PandaX-4T Commissioning Run," Phys. Rev. Lett. **127**, no.26, 261802 (2021).

[29] A. Arhrib, R. Benbrik, and N. Gaur, "$H \to \gamma\gamma$ in Inert Higgs Doublet Model," Phys. Rev. D **85**, 095021 (2012).

[30] A. Vicente and C. E. Yaguna, "Probing the scotogenic model with lepton flavor violating processes," JHEP **02**, 144 (2015).

[31] G. Aad et al. [ATLAS], "Searches for electroweak production of supersymmetric particles with compressed mass spectra in $\sqrt{s} = 13\,\text{TeV}$ pp collisions with the ATLAS detector," Phys. Rev. D **101**, no.5, 052005 (2020).

[32] A. M. Sirunyan et al. [CMS], "Search for supersymmetry in final states with two oppositely charged same-flavor leptons and missing transverse momentum in proton-proton collisions at $\sqrt{s} = 13\,\text{TeV}$," JHEP **04**, 123 (2021).